Near-Unity Singlet Fission on a Quantum Dot Initiated by Resonant Energy Transfer

Jie Zhang,[1] Hayato Sakai,*[2] Katsuaki Suzuki,[3] Taku Hasobe,[2] Nikolai V. Tkachenko,[4] I-Ya Chang,[5] Kim Hyeon-Deuk,[5] Hironori Kaji,[3] Toshiharu Teranishi,*[3] Masanori Sakamoto*[3]

[1]Department of Chemistry, Graduate School of Science, Kyoto University, Gokasho, Uji, Kyoto 611-0011, Japan

[2]Department of Chemistry, Faculty of Science and Technology, Keio University, 3-14-1 Hiyoshi, Kohoku-ku, Yokohama, Kanagawa 223-8522, Japan

[3]Institute for Chemical Research, Kyoto University, Gokasho, Uji, Kyoto 611-0011, Japan

[4]Chemistry and Advanced Materials Group, Faculty of Engineering and Natural Sciences, Tampere University, Korkeakoulunkatu 8, FI33720 Tampere, Finland

[5]Department of Chemistry, Kyoto University, Kyoto, Kyoto 606-8502, Japan

ABSTRACT: The conversion of a high-energy photon into two excitons using singlet fission (SF) stimulates a variety of studies in fields from fundamental physics to device applications. However, efficient SF has only been achieved in limited systems, such as solid crystals and covalent dimers. Here, we established a novel system by assembling 4-(6,13-bis(2-(triisopropylsilyl)-ethynyl)pentacene-2-yl)benzoic acid (Pc) chromophores on nano-sized CdTe quantum dots (QDs). A near-unity SF (198 ± 5.7%) initiated by interfacial resonant energy transfer from CdTe to surface Pc was obtained. The unique arrangement of Pc determined by the surface atomic configuration of QDs is the key factor realizing unity SF. The back reaction, triplet-triplet annihilation, was remarkably suppressed owing to the rapid dissociation of triplet pairs, leading to long-lived free triplets. In addition, the low light-harvesting ability of Pc in visible region was promoted by the efficient energy transfer (99 ± 5.8%) from QDs to Pc. The synergistically enhanced light-harvesting ability, high triplet yield and long-lived triplet lifetime of the SF system on nano-interfaces could pave the way for an unmatched advantage of SF.

INTRODUCTION

Singlet fission (SF) in organic chromophores is an exciton multiplication process in which a spin-singlet excited state splits into a pair of spin-triplet excited states[1-6]. The conversion of a high-energy photon into two photons/excitons by SF stimulates a variety of studies in fields from fundamental physics to solar energy conversion[7-11]. Because SF is an intra- and inter-bimolecular phenomenon that requires suitable intermolecular electronic coupling, investigations of SF have focused on organic materials with highly dense packing, such as crystalline solids, aggregates and extremely concentrated solutions[12-16]. In addition, covalently tethered dimers have been developed to optimize chromophore configurations for SF[17-22]. Earlier reports of SF suggested that controlling for intermolecular orientation and/or distance holds a key to achieving efficient SF[22-27]. Exploring an ideal system exhibiting a favourable molecular arrangement for SF is still challenging and strongly demanded.

An inorganic quantum dot (QD) surface is a promising platform for concentrating functional molecules in a limited region[28, 29]. QDs present an excellent light-harvesting property that can be systematically controlled by the size-dependent quantum confinement effect, providing intense absorptions and emissions ranging from the ultraviolet (UV) to the infrared

(IR) regions[30-32]. The versatile charge/energy transfer between QDs and surface-attached molecules suggests that QDs promote the light-harvesting ability of a whole system[33]. Therefore, composites of QDs and organic molecules can be an ideal system for establishing efficient SF. However, the favourable sensitization system (Förster resonance energy transfer or Dexter-like singlet energy transfer) for QD-molecule composite is still under debate[34,35]. Furthermore, the triplet yields by SF on previously reported QD-molecule systems have been far from the ideal value[34,35]. Even for the QD-molecular dimer systems employing the intramolecular SF, the triplet yield was 160%.[34] The triplet yield of the QD-molecular monomer systems (intermolecular SF system) (113%) initiated by Dexter-like energy transfer well below the value [35]. The construction of ideal systems based on the understanding of underlying mechanism and key factors has been strongly required.

Here, we successfully demonstrated an ideal composite for SF by assembling 4-(6,13-bis(2-(triisopropylsilyl)-ethynyl)pentacene-2-yl)benzoic acid (Pc) molecules on the surface of CdTe QDs. From the results of femtosecond transient absorption (fsTA) measurements, the triplet yield of the intermolecular SF system was determined to reach 199 ± 7.6%, which is the highest record among the QD-molecule systems. Furthermore, the total triplet yield of SF *via* fluorescence resonance energy transfer (FRET) was 198 ± 5.7% due to unity

energy transfer between Pc and QDs (99 ± 5.8%). Furthermore, recombination of triplet pairs was remarkably suppressed in the current system. These results suggested that the excitons generated in CdTe can be transferred to Pc and completely separated into two triplet excitons. A double-quantum (DQ) experiment using dynamic nuclear polarization enhanced nuclear magnetic resonance (DNP-NMR) and computational simulation unveiled the unique molecular arrangement of Pc dimer on CdTe QDs, reflecting the surface atomic configuration realized the efficient SF.
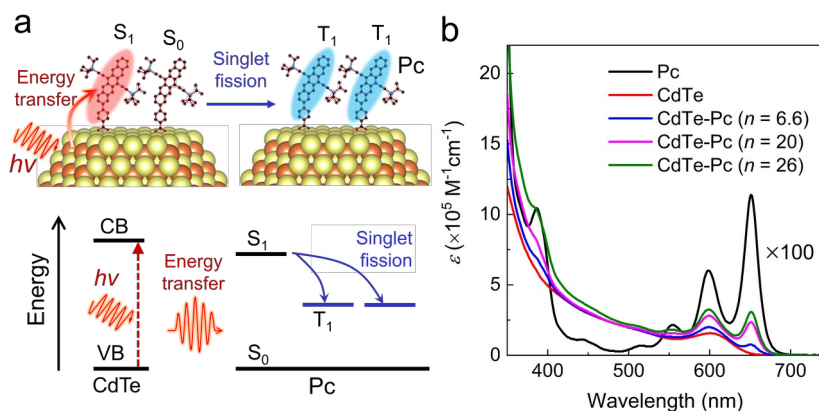

Figure 1. Schematic illustration and absorption spectra of the QD-molecule composite for SF. a, Schematic illustration of SF at the CdTe-Pc heterointerface. An exciton generated in a CdTe QD transfers to Pc, forming a molecular singlet exciton. Then, the singlet excited Pc molecule undergoes SF with a neighbouring molecule to produce two triplet excitons. b, UV–vis–near-IR absorption spectra of CdTe QDs, CdTe-Pc and Pc in toluene (n is the average number of Pc molecules on a single QD).

RESULTS

Materials design. A schematic of the QD-molecule composite and all the relevant photophysical processes is displayed in Figure 1a. CdTe QDs were selected as a scaffold for the QD-molecule system. Pc derivatives have been extensively investigated as SF chromophores because they cause rapid and efficient SF due to well-matched energy levels, $2E(T_1) \approx E(S_1)$, where $E(T_1)$ and $E(S_1)$ are the energy levels of the lowest triplet and lowest singlet excited states, respectively[1, 36]. Near-unity triplet yields have been achieved in solids and solutions of Pc derivatives[13, 37]. However, the light-harvesting ability of Pc derivatives is relatively low because of their extremely low absorption coefficients (ε) (16×10^3 M^{-1} cm^{-1} in the 400-500 nm range)[35]. In contrast, ε of CdTe QDs is ~ 2×10^5 M^{-1} cm^{-1} in the same range[31], approximately two orders of magnitude higher than that of Pc. To achieve an efficient FRET from QDs to Pc, the emission of QDs was controlled to overlap with the absorption of Pc at approximately 600 nm. The low absorption of Pc is covered by the absorption of CdTe, which promotes the efficiency of exciton generation in Pc against incident photons. The excitons generated in the CdTe QDs can transfer to Pc through FRET. SF from the excited singlet state of Pc produces a maximum of two triplet states.

Synthesis and characterization of samples. CdTe QDs were synthesized by a hot injection method and dissolved in toluene solution (see Supplementary Information, Section 1). Transmission electron microscopy (TEM) images indicate that the size of the CdTe QDs is 3.5 ± 0.3 nm (Figure S3). X-ray diffraction (XRD) patterns indicate that the crystal structure of the CdTe QDs is zinc blende (JCPDS 15-0770) (Figure S4). Pc molecules were assembled on QDs by a ligand exchange reaction. The carboxylic acid group attaches Pc to the CdTe surface. The average number of Pc on a single QD (n) is quantitatively controlled by changing the concentration of Pc

in the ligand exchange reaction. Three samples with different values of n of 6.6, 20, and 26 were prepared. UV–vis–near-IR absorption spectra of CdTe-Pc show the characteristic absorption features of Pc (555, 600, and 650 nm) and CdTe (600 nm) (Figure 1b). The value of n was calculated spectroscopically by comparing the concentrations of Pc and CdTe in the CdTe-Pc toluene solutions (see Supplementary Information, Section 4).

Femtosecond transient absorption measurements. fsTA measurements were conducted to observe the excited state dynamics of CdTe QDs and CdSe-Pc composites. Two excitation wavelengths were used, 470 and 660 nm, to excite predominantly QDs and Pc, respectively. Formation of composites is statistical in its nature, which complicates the TA data analysis. It is accepted that Poisson distribution can describe reasonably well the composite formation and this allows to use analytical expression to model QD exited state decay (see SI) [J. Phys. Chem. C (2009) Vol. 113, No 45, 19488-19492; J. Phys. Chem. C (2015) 119, 17561−17572] which will be called here "Poisson decay" for shortness. A sum of exponentials, Poisson decay and a step-function (f(t)=0 at t<0 and f(t)=1 at t>0) to fit globally two-dimensional fsTA data (depending on time and wavelength) and obtain so-called decay associated component spectra (DACS, see SI for details). The step function presents species which do not decay within the instrument time scan limit (roughly 5 ns).

The CdSe-Pc(n=26) sample can be fitted with three essential components, two exponentials with time constants 23 and 820 ps and step function. Assuming a linear reaction scheme (S1 → X → T) the spectra on the intermediate states were calculated and presented in Figure N1. The primary formed state is shown by the gree curve and assigned to the Pc singlet excited state. The longest-lived state (step function) is shown by the magenta, it is formed with 820 ps time constant and has

shape typical for the Pc triplet state [some reference]. There is an intermediate shown by the blue which is observed at a few hundreds ps. It may originate as the result of different Pc arrangements and aggregates on QD surface or be a coupled triplet state pair.
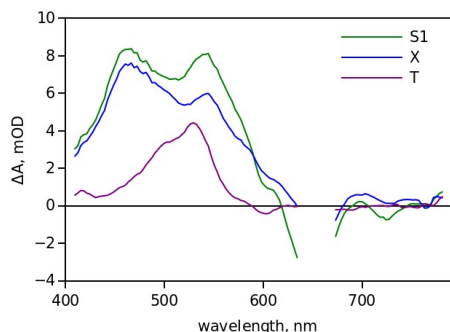

Figure N1. Species associated spectra of CdSe-Pc(n=26) after excitation at 660 nm.

The fit of QD samples requires constant accounting for the QD emission, a subsecond exponential component known to originated from the thermal relaxation of carriers at the conduction band [same references] and the Poisson component, as presented in Figure 2c. The essential component here is the Poisson one, which suggests rather long lifetime of the QD excited state (roughly 10 ns) and almost defect free QDs in the sample used (relative concentration of defects is 0.3).

The composite sample excited at 470 nm has the most complex relaxation dynamics (Figure 2d), but can be fitted successfully by combining two models, one used for QDs alone and another for composites excited at 660 nm. The resulting DACS are shown in Figure 2f, in which the the Poisson component has the same shape as that of QDs alone but in the case of composite sample it is dominated by quenching with time constant 110 ps. The exponential (530 ps) and step components are similar to those observed with excitation at 660 ps. Applying the same analysis the spectra of the intermediate states were calculated and presented in Figure N2. This shows that the relaxation of the QD excitation results in formation of the Pc singlet excited state, which decay to the triplet similarly to the case of direct excitation of Pc.
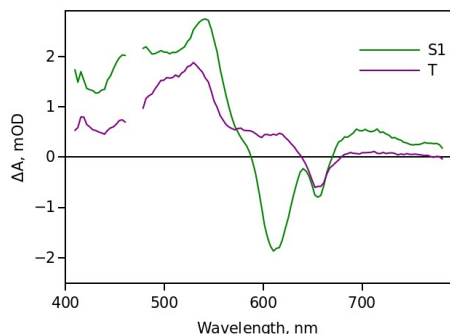
A two-dimensional (2D) fsTA map of the pristine CdTe QDs is displayed in Figure 2a. Upon excitation of the QDs by a 470 nm laser pulse, the 2D fsTA map is dominated by a strong negative signal at approximately 600 nm, which is attributed to the bleaching caused by the state filling of QDs induced by the transition of electrons from the valence to conduction band[38]. The photo-induced absorption at approximately 540 nm is derived from a transition from an excited state to a higher excited state or a biexcitonic state[39]. The recovery can be fitted by exponential growth functions (Figure 2b). The recovery of the ground-state bleaching is not complete within the time window of the fsTA system (5300 ps) (Figure 2b).

Figure N2. The singlet and triplet state spectra of Pc derived from the global analysis of DACS presented in Figure 2f.

Among the three CdTe-Pc samples, SF occurs most efficiently for that with $n = 26$. As shown in the fsTA spectrum of CdTe-Pc (Figure 2d), the CdTe QDs were selectively excited by the 470 nm laser pulse because the absorbed photon by Pc was negligible ($\sim$ 3%). The recovery of the ground-state bleaching is 8.9 $\times$ 10^9 s^{-1}, which is much faster than that of pristine QDs, suggesting that the excitons in the CdTe QDs are quenched by FRET to the surface Pc. The recovery of the bleaching is accompanied by two positive signals of excited-state absorption, which is characteristic of Pc in the singlet excited state (Pc (S_1)) light green line region in Figure 2d. Since the rate of increase in Pc (S_1) matches the recovery rate of the ground-state bleaching of the CdTe QDs, excitons generated in the CdTe QDs are transferred to Pc (S_1) *via* FRET. The possibility of carrier transfer was eliminated by the absence of the TA signal of Pc radical cations or anions. Finally, the TA signal assigned to the triplet state (Pc (T_1)) was observed (yellow line region in Figure 2d). Since the decay rate of Pc (S_1) and growth rate of Pc (T_1) were similar to each other (1.2 $\times$ 10^9 s^{-1}), we believe that SF generates Pc (T_1). Although it is plausible that the direct triplet energy transfer at the interface of CdTe-Pc can also form Pc (T_1), this process can be eliminated by the formation of Pc (S_1) before the formation of Pc (T_1). The time-resolved shift of TA confirmed that sequential FRET and SF occurred on CdTe-Pc.
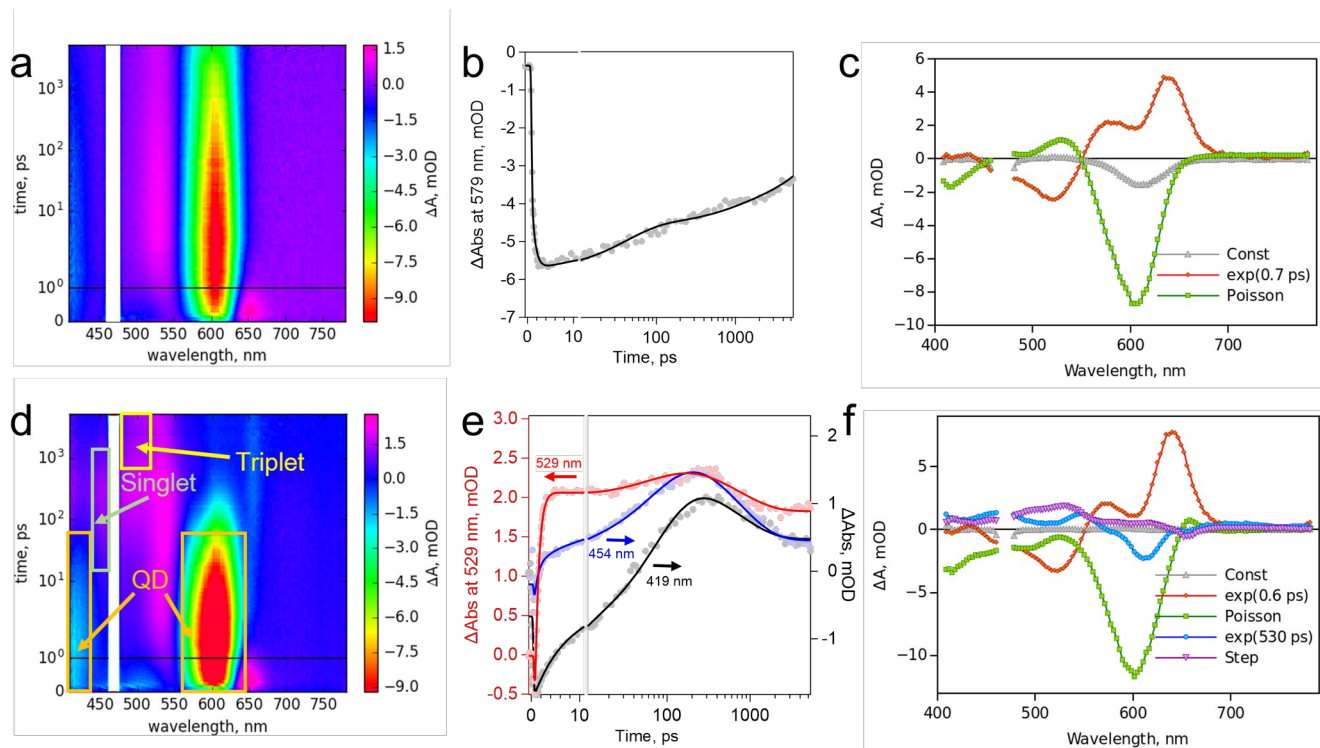
Figure 2. fsTA spectra of CdTe QDs and CdTe-Pc pumped at 470 nm. a, 2D fsTA maps of CdTe QDs. b, Kinetic profiles of CdTe QDs. The profiles are fitted by multi-exponential growth functions and the function described by a kinetic model assuming a Poisson distribution of adsorbates on quantum dots. First component was extracted by exponential fitting, and second component was extracted by the decay model utilizing the Poisson distribution. The solid line is the best fit. d, 2D fsTA maps of CdTe-Pc ($n = 26$). Bleaching of QDs is quenched by energy transfer from CdTe to Pc (orange line region near 600 nm), accompanied by components of singlet Pc (light green line region near 454 nm) and triplet Pc (yellow line region near 529 nm). e, Kinetic profiles of CdTe-Pc ($n = 26$). The profiles are fitted by multi-exponential growth functions and function described by a kinetic model assuming a Poisson distribution of adsorbates on quantum dots. First, third, and final components were extracted by exponential fitting, and second component was extracted by the decay model utilizing the Poisson distribution. The solid lines are the best fits. c, f, Global fitting analysis for the TA spectra in a (c) (const : the constant of fitting function, exp(0.4 ps) : the component of time constant of 0.7 ps assigned to be CdTe QD by exponential function, poisson : the component of poisson distribution) and d (f) (const : the constant of fitting function, exp(0.6 ps) : the component of time constant of 0.6 ps assigned to be CdTe QD by exponential function, poisson : the component of poisson distribution, the component of time constant of 530 ps assigned to be Pc(S$_1$) by exponential function, and step : the component of time constant of long-lived lifetime assigned to be Pc(T$_1$) by exponential function.). The values in the inset are time constant.

To obtain more insight into the relaxation mechanism, time profiles at all wavelengths were generated by a global fitting analysis using a multi-exponential function and the function based on Poisson distribution. Through the global analysis shown in Figure 2c, it is deduced that there are three evolution associated spectra (EAS) with different lifetimes for the QDs. The component with a very short lifetime 0.7 ps (red) is thermal relaxation of QDs to the lowest excited state. The EAS, with a lifetime component of 90 ps (green) determined by the function based on Poisson distribution[40-42], exhibiting the multistep recovery of the bleaching of the CdTe QDs, correspond to the high-energy exciton state, exciton state, and defect trapping state, respectively[38, 39]. In the global fitting analysis shown in Figure 2f, five EAS suggest the process of SF *via* FRET on CdTe-Pc. The EAS of CdTe-Pc with a lifetime component of 0.6 (red) is thermal relaxation of QDs, and a lifetime component of the decay model utilizing the Poisson distribution (green) is 90 ps. Although the quenching time constant is rather similar to that observed in CdTe QDs, this value is a different process because the concentration of quenchers in CdTe-Pc is ten times greater than that of pristine QD, which shows the energy transfer from QDs to Pc. Then, the EAS with a time constant of 530 ps (blue) is assigned to

mainly component of Pc (S$_1$) with unique peaks at 454 and 540 nm. The next EAS with a time constant of >5300 ps (purple) corresponds to Pc (T$_1$). This time-resolved shift of TA signals further identifies the occurrence of FRET and SF between Pc molecules on the surface of QDs. The quantum yield of FRET and the triplet yield of SF *via* FRET were calculated to be 99 ± 5.8 % and 198 ± 5.7%, respectively (see Method for details). As the triplet yield was the same as the value (199 ± 7.6%) of SF that occurred by selectively exciting only Pc with a 660 nm laser, the observed triplet states are generated by only SF. Therefore, the kinetic constant of SF was determined to be 1.2 × 10^9 s^{-1} from this pump-probe spectra. The near-unity quantum yield of FRET could be ascribed to the excellent overlap between the emission of CdTe and the absorption of Pc. The calculated triplet yield of 198 ± 5.7% (SF efficiency: 99 ± 5.8%) indicates that the CdTe-Pc composite could achieve SF with near-unity efficiency. The other QD systems also evaluated the yields and the dynamics by using the same method. The near unity SF efficiency of the current CdTe-Pc system was also supported by the time resolved fluorescence measurement (see Supplementary Information, Section 9).[43]

DISCUSSION

The importance of the intermolecular distance and morphology of SF chromophores for SF has been extensively demonstrated[23-25, 44]. The occurrence of SF requires a short intermolecular distance of Pc ($\stackrel{\circ}{\sim}$ 1 nm) for intermolecular electronic coupling[36, 37]. To investigate the effect of the average in-

termolecular distance on the SF rate and triplet yield, we changed the intermolecular distance (i.e., surface Pc density) of the surface-attached Pc by changing n. The parameters expressing the average distance of Pc on CdTe and the properties of SF are shown in Table 1 (Supplementary Information, Sections 4 and 5).

Table 1. Parameters of the QD-Pc composites and properties of SF.

Sample	n	Density (nm^{-2})	Distance (nm)	FRET yield (%)	SF rate (ns^{-1})	Triplet yield (%)
CdTe-Pc	6.6	0.31	1.8	87 ± 5.9	0	0
	20	0.95	1.0	95 ± 5.1	0.71	159 ± 6.8
	26	1.2	0.90	99 ± 5.8	1.2	198 ± 5.7
CdTe@CdS-Pc	30	0.65	1.3	93 ± 9.9	0	0

CdTe-Pc with a small number of Pc (n = 6.6) has a surface Pc density of 0.31 nm^{-2} and an average intermolecular distance of 1.8 nm. As shown in Table 1 and Figure S8, excitons generated in QDs successfully transferred to the singlet states of Pc with a quantum yield of 87 ± 5.9%. However, no triplet signal was observed from the TA spectra of CdTe-Pc (n = 6.6), suggesting that SF did not occur in the composite with the small n value. This finding could be ascribed to the intermolecular distance of 1.8 nm, which is too long to produce electronic coupling between surface Pc molecules. This result also confirmed that direct triplet energy transfer does not occur in the CdTe-Pc (n = 6.6) system. As the intermolecular distance decreased from 1.8 nm to 1.0 nm, the triplet yield reached 159 ± 6.8% for CdTe-Pc (n = 20).

To confirm the hypothesis that the intermolecular distance of Pc on a QD holds a key to SF, we further investigated the effect of the surface Pc density on SF by synthesizing CdTe@CdS core@shell. In the core@shell system, we can change only the surface area of QDs without significant changes in n and the optical properties of QDs. We realized a first absorption peak at 600 nm for the CdTe@CdS QDs similar to that of the CdTe QDs, while the size of CdTe@CdS (5.4 nm) was larger than that of CdTe (3.5 nm). Although n in CdTe@CdS increased to 30, the surface Pc density decreased to 0.65 nm^{-2}, leading to a longer intermolecular distance (1.3 nm). FRET occurred from CdTe@CdS to the surface Pc, but no SF was observed, clearly demonstrating that the intermolecular distance is a key parameter to provide favourable intermolecular coupling for SF.

The NMR method can also provide information on ^{13}C-^{13}C correlation between Pc ligands by employing a homonuclear recoupling technique[45, 46] (Figure 3a), which can estimate dipole–dipole coupling between nuclei of interest. However, the intrinsic low sensitivity of NMR prevents the application of such measurements for natural abundance samples. In this work, to enhance the sensitivity of NMR, we used a dynamic nuclear polarization (DNP) method[47-52]. DNP-enhanced ^{13}C cross-polarization (CP) magic angle spinning (MAS) spectrum

of CdTe-Pc (n = 26) showed ca. 13 times signal enhancement (Figure 3b).

On the basis of this result, 2D ^{13}C-^{13}C dipolar DQ correlation spectra were recorded using the SPC5 homonuclear recoupling sequence (Figure 3a). For both samples, a correlation peak was observed at approximately 38 ppm, corresponding to ^{13}C in CH$_3$ and CH groups in the isopropyl (i-Pr) units (Figure 3b), indicating that CH$_3$-CH$_3$ and CH$_3$-CH are in close proximity. To obtain further insight, the DQ efficiency buildup curves were recorded (Figure 3d). At short excitation times, the DQ efficiencies were similar for both samples. The main contribution for the DQ efficiencies at short times is intramolecular CH$_3$-CH$_3$ and CH$_3$-CH coupling in the i-Pr unit. The difference of DQ efficiencies between CdTe-Pc with n = 26 and 6.6 value become larger with increasing the excitation time, indicating the significant contribution of intermolecular dipole-dipole coupling for CdTe-Pc with a high n value of 26. The n dependence of DQ efficiency build-up curve indicates that the observed signal corresponds to the intermolecular interaction between Pc on a QD. These results are in good agreement with the results of fsTA spectra. The computational simulation of DQ buildup curve suggested that the major distance of intermolecular CH$_3$ in the i-Pr unit is around 4 Å (Figure S16).
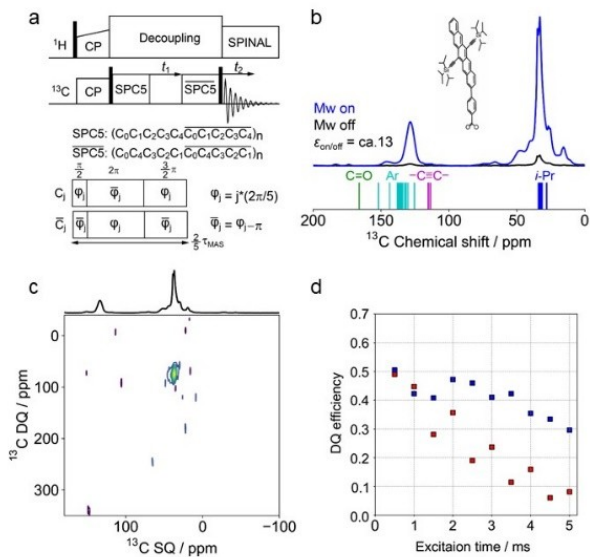
Figure 3. DNP-NMR measurements of CdTe-Pc. a, SPC5 Pulse sequence for 2D ^{13}C-^{13}C DQ dipolar correlation spectra[42]. b, ^{13}C CP/MAS spectra of CdTe-Pc (n = 26) with and without microwave irradiation. c, 2D ^{13}C-^{13}C DQ dipolar correlation spectra

of CdTe-Pc (n = 26). The spectrum was recorded using a DQ excitation time of 0.5 ms, 64 t_1 increments and 128 repetitions for each t_1 increment. The repetition delay was 4 s. d, DQ buildup curves for CdTe-Pc (n = 26) (blue square) and CdTe-Pc (n = 6.6) (red square).

The computational method predicted the most likely arrangement of Pc dimer on a CdTe surface. As the nearest-neighbour arrangement of Pc dimer, we consider the parallel and anti-parallel configurations of Pc on a CdTe(111) surface as a representative facet of QD (Figure 4 and supplementary information). From the results of the geometrical optimization, the two Pc stably coordinated on the CdTe(111) surface by the parallel or anti-parallel configuration. The intermolecular distance and shift length between Pc are estimated to be ~8.7 Å and ~4.2 Å, respectively, in the both configurations. The intermolecular distance is 8.7 Å, which agrees with 9 Å estimated from the surface density of Pc, realizes the present efficient SF. The deviation of Pc molecular faces, 4.2 Å, is larger than that reported in the crystalline solid of pentecene[24]. The unique molecular
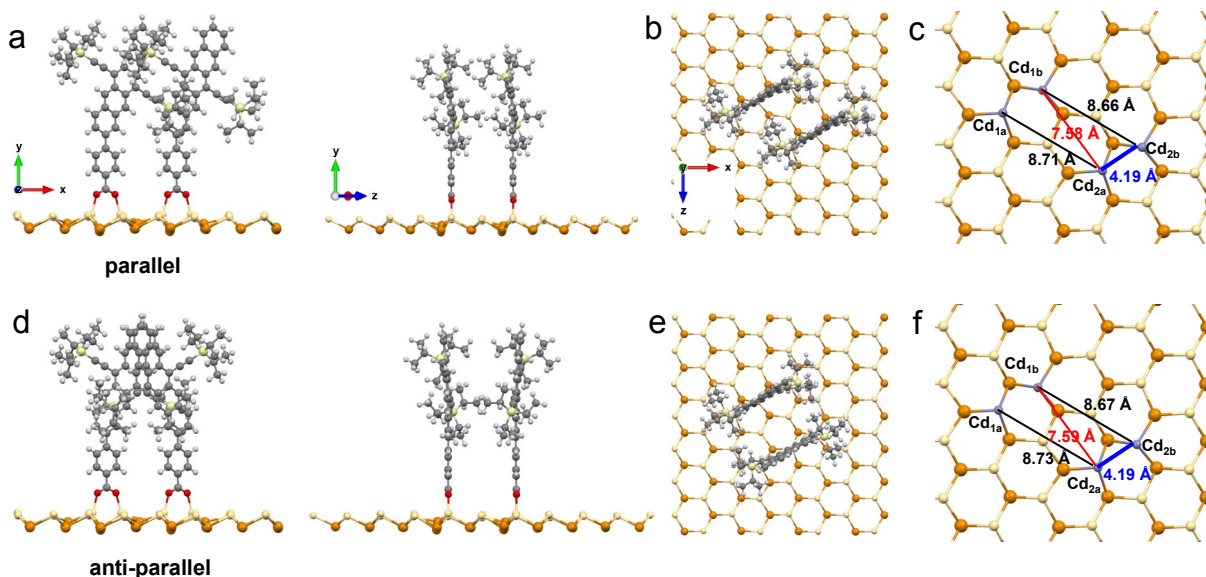

Figure 4. Computed molecular configurations of Pc on a CdTe surface. The parallel (a) and anti-parallel (d) configurations of Pc dimer after geometrical optimization. The corresponding top views of the parallel and anti-parallel configurations are given in (b) and (e), respectively. Atomic arrangements of CdTe(111) directly related to the intermolecular distance of Pc dimer with the parallel (c) and anti-parallel (f) configurations. The black values correspond to the intermolecular direct distance between the Pc molecular faces, while the red values are orthogonal intermolecular distance between two parallel planes where each Pc molecular plane exists. The parallel deviation of paired Pc molecules (blue values) can be calculated through Pythagorean theorem.

arrangement of the Pc pair was determined by the atomic arrangement of CdTe(111) because of the coordination between the carboxylic acid group and the Cd atom.

The computed total energy of the parallel configuration is 0.031 eV lower than that of the anti-parallel configuration, indicating that the parallel configuration is more preferred than the anti-parallel configuration. In fact, the intermolecular CH$_3$-CH$_3$ distance in the i-Pr unit indicated by DNP-NMR, ~4.0 Å, well-agreed with the value of 4.5 Å estimated in the optimized parallel configuration (Figures 4a and 4b). Furthermore, the molecular orbital calculation indicated the partial intermolecular delocalization of molecular orbitals of Pc only in the parallel configuration owing to its larger overlapping area of Pc molecular face, which should be favourable for SF (Figure S17). Therefore, we conclude that the increase of n leads to the formation of the parallel Pc dimer resulting in the dramatic increase of SF efficiency.

The DNP-NMR and computational calculation indicated that the configuration of Pc is determined by the atomic arrangement of the CdTe(111) surface. The CdTe(111) surface structure promotes to build the parallel and largely mismatched Pc dimer, which has not been reported in any conventional systems. The unique molecular arrangement, which was

achieved owing to the stable attachment of Pc-pairs on the CdTe(111) surface, realized the current near-unity SF.

The arrangement of chromophores also plays an important role in controlling the dissociation and recombination of free triplets. An investigation of SF dimers demonstrated that strongly conjugated molecules led to radiative recombination and other competitive processes to free triplets, reducing triplet yield and lifetime[22]. Thus, a unity SF efficiency can be obtained by dimers, but the corresponding triplet lifetime is short because the diffusion of free triplets is prohibited in an SF system with a small number of molecules[17]. Achieving balanced intermolecular coupling is the key to efficient SF and is challenging. Nanosecond transient absorption (nsTA) spectra show that Pc (T_1) generated on the surface of CdTe QDs has a long lifetime (~30 μs) (Figure S15) that is longer than the previously reported values for crystalline solids and covalent dimers of pentacene[17, 53]. From the result of kinetic analysis of decay profile of Pc(T_1), the decay corresponding to the back reaction (*i.e.* triplet-triplet annihilation) was negligible (0.2%). The estimated triplet yield of SF from the long-lived component of ns-TAS was 184%, indicating that almost no back reaction occurred even in the ms region. Since no signals of Pc aggregation were observed in the spectroscopic investigation, we believe that the interaction between Pc molecules is negligible on the QD surface[13]. Such a non-conjugated arrangement of Pc on the surface of CdTe provides a through-space interaction for SF, which will prevent undesired deactivation processes. The Pc on QD exquisitely gather for the efficient dissociation and maintain of free triplets.

CONCLUSION

We have demonstrated that the composition of QD and molecules provide an important option for designing the ideal SF systems. CdTe QD is an excellent scaffold from the viewpoint of compensation of weak light-harvesting ability of Pc, and specific arrangements of surface attached Pc molecules in improving the triplet yield and lifetime of SF.

The unique properties of Pc configured on the nano-interfaces and synergy with QDs could expand the possibilities of SF for a variety of applications, including minuscule optical devices, energy devices, and photo-energy conversion.

ASSOCIATED CONTENT

Supporting Information.
The Supporting Information is available free of charge on the ACS publications website at DOI: XXX
Experimental procedures, figures, and corresponding discussions of additional supporting experimental data

AUTHOR INFORMATION

Corresponding Author

*sakamoto@scl.kyoto-u.ac.jp
*sakai@chem.keio.ac.jp
*teranisi@scl.kyoto-u.ac.jp

ORCID
Jie Zhang: 0000-0002-3079-0977
Taku Hasobe: 0000-0002-4728-9767
Nikolai V. Tkachenko: 0000-0002-8504-2335
Kim Hyeon-Deuk: 0000-0002-5815-8041
Hironori Kaji: 0000-0002-5111-3852
Toshiharu Teranishi: 0000-0002-5818-8865
Masanori Sakamoto: 0000-0001-5018-5590

REFERENCES

1. Smith, M. B. & Michl, J. Singlet fission. *Chem. Rev.* **110,** 6891-6936 (2010).
2. Johnson, J. C., Nozik, A. J. & Michl, J. High triplet yield from singlet fission in a thin film of 1,3-Diphenylisobenzofuran. *J. Am. Chem. Soc.* **132,** 16302-16303 (2010).
3. Kato, D., Sakai, H., Tkachenko, N. V. & Hasobe, T. High-yield excited triplet States in pentacene self-assembled monolayers on gold nanoparticles through singlet exciton fission. *Angew. Chem. Int. Ed.* **55,** 5230-5234 (2016).
4. Sakai, H. et al. Multiexciton dynamics depending on intramolecular orientations in pentacene dimers: recombination and dissociation of correlated triplet pairs. *J. Phys. Chem. Lett.* **9,** 3354-3360 (2018).
5. Miyata, K., Conrad-Burton, F. S., Geyer, F. L. & Zhu, X. Y. Triplet pair states in singlet fission. *Chem. Rev.* **119,** 4261-4292 (2019).
6. Saegusa, T. et al. Controlled orientations of neighboring tetracene units by mixed self-assembled monolayers on gold nanoclusters for high-yield and long-lived triplet excited states through singlet fission. *J. Am. Chem. Soc.* **141,** 14720-14727 (2019).
7. Hanna, M. C. & Nozik, A. J. Solar conversion efficiency of photovoltaic and photoelectrolysis cells with carrier multiplication absorbers. *J. Appl. Phys.* **100,** 074510 (2006).
8. Ehrler, B., Wilson, M. W. B., Rao, A., Friend, R. H. & Greenham, N. C. Singlet exciton fission-sensitized infrared quantum dot solar cells. *Nano Lett.* **12,** 1053-1057 (2012).
9. Congreve, D. N. et al. External quantum efficiency above 100% in a singlet-exciton-fission-based organic photovoltaic cell. *Science* **340,** 334-337 (2013).
10. Einzinger, M. et al. Sensitization of silicon by singlet exciton fission in tetracene. *Nature* **571,** 90-94 (2019).
11. Kunzmann, A. et al. Singlet fission for photovoltaics with 130% injection efficiency. *Angew. Chem. Int. Ed.* **57,** 10742-10747 (2018).
12. Wilson, M. W. B. et al. Ultrafast dynamics of exciton fission in polycrystalline pentacene. *J. Am. Chem. Soc.* **133,** 11830-11833 (2011).
13. Walker, B. J., Musser, A. J., Beljonne, D. & Friend, R. H. Singlet exciton fission in solution. *Nat. Chem.* **5,** 1019-1024 (2013).
14. Pensack, R. D. et al. Solution-processable, crystalline material for quantitative singlet fission. *Mater. Horiz.* **4,** 915-923 (2017).
15. Pensack, R. D. et al. Striking the right balance of intermolecular coupling for high-efficiency singlet fission. *Chem. Sci.* **9,** 6240-6259 (2018).
16. Jones, A. C., Kearns, N. M., Ho, J. J., Flach, J. T. & Zanni, M. T. Impact of non-equilibrium molecular packings on singlet fission in microcrystals observed using 2D white-light microscopy. *Nat. Chem.* **12,** 40-47 (2020).
17. Sanders, S. N. et al. Quantitative intramolecular singlet fission in bipentacenes. *J. Am. Chem. Soc.* **137,** 8965-8972 (2015).

18. Zirzlmeier, J. et al. Singlet fission in pentacene dimers. *Proc. Natl Acad. Sci. USA* **112,** 5325-5330 (2015).

19. Sakuma, T. et al. Long-lived triplet excited states of bent-shaped pentacene dimers by intramolecular singlet fission. *J. Phys. Chem. A* **120,** 1867-1875 (2016).

20. Kumarasamy, E. et al. Tuning singlet fission in pi-bridge-pi chromophores. *J. Am. Chem. Soc.* **139,** 12488-12494 (2017).

21. Basel, B. S. et al. Unified model for singlet fission within a non-conjugated covalent pentacene dimer. *Nat. Commun.* **8,** 15171 (2017).

22. Pun, A. B. et al. Ultra-fast intramolecular singlet fission to persistent multiexcitons by molecular design. *Nat. Chem.* **11,** 821-828 (2019).

23. Johnson, J. C., Nozik, A. J. & Michl, J. The role of chromophore coupling in singlet fission. *Acc. Chem. Res.* **46,** 1290-1299 (2013).

24. Wang, L. J., Olivier, Y., Prezhdo, O. V. & Beljonne, D. Maximizing singlet fission by intermolecular packing. *J. Phys. Chem. Lett.* **5,** 3345-3353 (2014).

25. Wu, Y. S. et al. Impact of intermolecular distance on singlet fission in a series of TIPS pentacene compounds. *J. Phys. Chem. Lett.* **5,** 3451-3455 (2014).

26. Tayebjee, M. J. Y. et al. Quintet multiexciton dynamics in singlet fission. *Nat. Phys.* **13,** 182-188 (2017).

27. Yablon, L. M. et al. Persistent multiexcitons from polymers with pendent pentacenes. *J. Am. Chem. Soc.* **141,** 9564-9569 (2019).

28. Anderson, N. C., Hendricks, M. P., Choi, J. J. & Owen, J. S. Ligand exchange and the stoichiometry of metal chalcogenide nanocrystals: spectroscopic observation of facile metal-carboxylate displacement and binding. *J. Am. Chem. Soc.* **135,** 18536-18548 (2013).

29. Boles, M. A., Ling, D., Hyeon, T. & Talapin, D. V. The surface science of nanocrystals. *Nat. Mater.* **15,** 141-153 (2016).

30. Murray, C. B., Norris, D. J. & Bawendi, M. G. Synthesis and characterization of nearly monodisperse CdE (E = S, Se, Te) semiconductor nanocrystallites. *J. Am. Chem. Soc.* **115,** 8706-8715 (1993).

31. Yu, W. W., Qu, L. H., Guo, W. Z. & Peng, X. G. Experimental determination of the extinction coefficient of CdTe, CdSe, and CdS nanocrystals. *Chem. Mater.* **15,** 2854-2860 (2003).

32. Lu, H. P., Carroll, G. M., Neale, N. R. & Beard, M. C. Infrared quantum dots: progress, challenges, and opportunities. *ACS Nano* **13,** 939-953 (2019).

33. Harris, R. D. et al. Electronic processes within quantum dot-molecule complexes. *Chem. Rev.* **116,** 12865-12919 (2016).

34. Sakai, H., Inaya, R., Tkachenko, N. V. & Hasobe, T. High-yield generation of triplet excited states by an efficient sequential photoinduced process from energy transfer to singlet fission in pentacene-modified CdSe/ZnS quantum dots. *Chem. Eur. J.* **24,** 17062-17071 (2018).

35. Lu, H. P., Chen, X. H., Anthony, J. E., Johnson, J. C. & Beard, M. C. Sensitizing singlet fission with perovskite nanocrystals. *J. Am. Chem. Soc.* **141,** 4919-4927 (2019).

36. Zimmerman, P. M., Zhang, Z. Y. & Musgrave, C. B. Singlet fission in pentacene through multi-exciton quantum states. *Nat. Chem.* **2,** 648-652 (2010).

37. Yost, S. R. et al. A transferable model for singlet-fission kinetics. *Nat. Chem.* **6,** 492-497 (2014).

38. Pietryga, J. M. et al. Spectroscopic and device aspects of nanocrystal quantum dots. *Chem. Rev.* **116,** 10513-10622 (2016).

39. Tyagi, P. & Kambhampati, P. False multiple exciton recombination and multiple exciton generation signals in semiconductor quantum dots arise from surface charge trapping. *J. Chem. Phys.* **134,** 094706 (2011).

40. Huang, J. E., Huang, Z. Q., Jin, S. Y., Lian, T. Q. Exciton dissociation in CdSe quantum dots by hole transfer to phenothiazine. *J. Phys. Chem. C* **112,** 19734-19738 (2008).

41. Sadhu, S., Tachiya, M., Patra, A. A stochastic model for energy transfer from CdS quantum dots/rods (donors) to Nile Red dye (acceptors). *J. Phys. Chem. C* **113,** 19488−19492 (2009).

42. Virkki, K., Demir, S., Lemmetyinen, H., Tkachenko, N. V. Photoinduced electron transfer in CdSe/ZnS quantum dot−fullerene hybrids. *J. Phys. Chem. C* **119,** 17561−17562 (2015).

43. Nakagawa, T., Okamoto, K., Hanada, H., Katoh, R. Probing with Randomly Interleaved Pulse Train Bridges the Gap between Ultrafast Pump-probe and Nanosecond Flash Photolysis. *Opt. Lett.* **41,** 1498-501, (2016).

44. Pensack, R. D. et al. Exciton delocalization drives rapid singlet fission in nanoparticles of acene derivatives. *J. Am. Chem. Soc.* **137,** 6790-6803 (2015).

45. Hohwy, M., Rienstra, C. M., Jaroniec, C. P. & Griffin, R. G. Fivefold symmetric homonuclear dipolar recoupling in rotating solids: application to double quantum spectroscopy. *J. Chem. Phys.* **110,** 7983-7992 (1999).

46. Karlsson, T., Popham, J. M., Long, J. R., Oyler, N. & Drobny, G. P. A study of homonuclear dipolar recoupling pulse sequences in solid-state nuclear magnetic resonance. *J. Am. Chem. Soc.* **125,** 7394-7407 (2003).

47. Overhauser, A. W. Polarization of nuclei in metals. *Phys. Rev.* **92,** 411-415 (1953).

48. Carver, T. R. & Slichter, C. P. Experimental verification of the Overhauser nuclear polarization effect. *Phys. Rev.* **102,** 975-981 (1956).

49. Hall, D. A. et al. Polarization-enhanced NMR spectroscopy of biomolecules in frozen solution. *Science* **276,** 930-932 (1997).

50. Ni, Q. Z. et al. High frequency dynamic nuclear polarization. *Acc. Chem. Res.* **46,** 1933-1941 (2013).

51. Rossini, A. J. et al. Dynamic nuclear polarization surface enhanced NMR spectroscopy. *Acc. Chem. Res.* **46,** 1942-1951 (2013).

52. Thankamony, A. S. L., Wittmann, J. J., Kaushik, M. & Corzilius, B. Dynamic nuclear polarization for sensitivity enhancement in modern solid-state NMR. *Prog. Nucl. Magn. Res. Sp.* **102,** 120-195 (2017).

53. Grieco, C., Doucette, G. S., Pensack, R. D., Payne, M. M., Rimshaw, A., Scholes, G. D., Anthony, J. E., Asbury, J. B. Dynamic exchange during triplet transport in nanocrystalline TIPS-pentacene films. *J. Am. Chem. Soc.* **138,** 16069-16080 (2016).